Perovskite Solar Cells

DOI: 10.1002/anie.201309361

Mixed-Organic-Cation Perovskite Photovoltaics for Enhanced Solar-Light Harvesting**

*Norman Pellet, Peng Gao, Giuliano Gregori, Tae-Youl Yang, Mohammad K. Nazeeruddin, Joachim Maier, and Michael Grätzel**

Abstract: *Hybrid organic–inorganic lead halide perovskite $APbX_3$ pigments, such as methylammonium lead iodide, have recently emerged as excellent light harvesters in solid-state mesoscopic solar cells. An important target for the further improvement of the performance of perovskite-based photovoltaics is to extend their optical-absorption onset further into the red to enhance solar-light harvesting. Herein, we show that this goal can be reached by using a mixture of formamidinium ($HN=CHNH_3^+$, FA) and methylammonium ($CH_3NH_3^+$, MA) cations in the A position of the $APbI_3$ perovskite structure. This combination leads to an enhanced short-circuit current and thus superior devices to those based on only $CH_3NH_3^+$. This concept has not been applied previously in perovskite-based solar cells. It shows great potential as a versatile tool to tune the structural, electrical, and optoelectronic properties of the light-harvesting materials.*

The large family of inorganic halometallate perovskites has attracted a lot of attention owing to its wide range of outstanding properties, such as antiferromagnetism,[1–3] photoconductivity,[4,5] ionic conductivity,[6] and bipolar semiconductivity.[7] Within this family, the fully inorganic cesium–metal–trihalide perovskites ($CsAX_3$, X = Cl, Br, I) have been the subject of intense study for many years.[8–17] In particular, organic–inorganic iodoplumbate and iodostannate perovskites, pioneered by Mitzi et al.,[18] have been recognized for their excellent semiconducting properties.[19] However, the extraordinary photovoltaic performance of similar hybrid perovskites only became evident after the demonstration of $MAPbI_3$ nanoparticles as potent light harvesters in a liquid-electrolyte-based dye-sensitized solar-cell configuration by Miyasaka and co-workers,[20] who observed a power-conversion efficiency (PCE) of 3.9%. A drawback of this system is its poor stability, as the perovskite rapidly degrades owing to its high solubility in the liquid electrolyte. This problem was overcome by replacing the electrolyte with a solid organic hole conductor.[21–27] Recently, we reported a new record of 15% PCE for a FTO/TiO_2/$MAPbI_3$/spiro-MeOTAD/Au device in which the perovskite was deposited by a novel sequential deposition technique.[23] By using our two-step deposition technique, we witnessed a significant increase in the open-circuit voltage (V_{oc}) and fill factor (FF) of our devices as compared to devices prepared by the commonly used one-step deposition method from γ-butyrolactone.[20,24,26,27] However, the short-circuit photocurrent density (J_{sc}) was limited to an average value of 17 mA cm^{-2}. In theory, a semiconductor with a band gap of 1.5 eV can deliver photocurrents up to 27 mA cm^{-2} under standard AM1.5G illumination. The large difference arises mainly from the lack of light absorption in the 550–800 nm range by the infiltrated perovskite and the parasitic absorption of the conductive oxide glass.

Hybrid organic–inorganic perovskites are synthesized with a variety of organic cations.[26,28–34] It has been demonstrated that the size of the organic ammonium cation influences the optical band gap of the perovskite by affecting the M-I-M (M = Sn, Pb) angle[35] or promoting the formation of insulating barriers between semiconducting PbI_4 layers.[30] In the latter case, bigger cations usually lead to two-dimensional perovskite, in which the PbI_6^{4-} octahedrons are edge-sharing. Two-dimensional (2D) iodoplumbate and iodostannate perovskites usually show wider band gaps,[36,37] which make them unsuitable for panchromatic absorption of the visible solar spectrum. A variety of organic cations have been shown to affect the band gap by as much as 1 eV in iodostannate perovskites.[36] Theoretically, methylammonium (CH_3NH_3, MA^+) and formamidinium ($HN=CHNH_3^+$, FA^+) are sufficiently small cations to form the 3D perovskite, whereas ethylammonium ($CH_3CH_2NH_3^+$) is known to already form a 2D perovskite.[26] $FASnI_3$ has been described by Mitzi and co-workers as early as 1995,[31] whereas its Pb analogue was only recently investigated by Kanatzidis and co-workers,[38] who reported a significant red shift of the optical absorption as compared to that of $MAPbI_3$. We reasoned that formamidinium offers the potential to lower the band gap of

[*] N. Pellet, Dr. P. Gao, Dr. M. K. Nazeeruddin, Prof. M. Grätzel
Laboratory of Photonics and Interfaces, Department of Chemistry and Chemical Engineering, Swiss Federal Institute of Technology Station 6, 1015 Lausanne (Switzerland)
E-mail: michael.graetzel@epfl.ch
N. Pellet, Dr. G. Gregori, Dr. T.-Y. Yang, Prof. J. Maier, Prof. M. Grätzel
Max-Planck-Institute for Solid-State Research
Heisenbergstrasse 1, 70569 Stuttgart (Germany)

[**] We thank K. Schenk for the XRD characterization, P. Labouchère for the SEM micrographs, and R. Humphry-Baker for fruitful discussions. We acknowledge financial support from Aisin Cosmos R&D Co., Ltd (Japan); the European Union Seventh Framework Program (FP7/2007–2013) under grant agreement "ENERGY-261920, ESCORT"; NANOMATCELL, grant agreement no. 308997; and the CCEM-CH in the 5th call proposal (DURSOL). M.G. thanks the Max Planck Society for a Max Planck Fellowship at the MPI for Solid State Research in Stuttgart (Germany); the King Abdulaziz University, Jeddah and the Nanyang Technolocal University, Singapore for Adjunct Professor appointments; and the European Research Council for an Advanced Research Grant (ARG 247404) funded under the "Mesolight" project.

Supporting information for this article is available on the WWW under http://dx.doi.org/10.1002/anie.201309361.

the commonly used $MAPbI_3$ perovskite towards the value of 1.4 eV,[39] which is optimal for the conversion of standard AM1.5 sunlight into electricity. We were able to tune the band gap of $MAPbI_3$ by the gradual substitution of MA with FA cations, and monitored the shift in the optical response. Earlier studies on mixed-cation perovskites focused on their electronic properties. Thus, Mitzi and co-workers described a semiconductor-to-metal transition within the series $(HN=CHNH_3)_2(CH_3NH_3)_nSn_nI_{3n+2}$[31,40] as n increased. Three-dimensional perovskites with mixed cations have also been prepared in the form of tin halide perovskites, that is, $(HN=CHNH_3)_{0.5}(CH_3NH_3)_{0.5}SnI_3$;[41] however, their optical or photovoltaic properties were not studied. Investigations to tune the band gap of metal halide perovskites have so far focused on the mixing of halide anions, for example, Br/I[37,42] or Cl/I,[3,33] rather than the use of mixed cations.

Herein we report the first use of 3D perovskites of composition $(MA)_x(FA)_{1-x}PbI_3$ ($x=0$–1) as light-harvesting pigments for mesoscopic solar cells. Our previously reported sequential deposition method[23] was used as a powerful and effective tool to generate perovskite crystals containing both methylammonium and formamidinium cations in well-defined proportions. We characterized the perovskite films by powder X-ray diffraction, AC and DC electrical conductivity (using carbon electrodes), absorption and emission spectroscopy, and photoluminescence decay. We tested fully functional photovoltaic (PV) devices with 2,2′,7,7′-tetrakis(*N*,*N*-di-*p*-methoxyphenylamine)-9,9′-spirobifluorene (spiro-OMeTAD) as the hole-transporting material (HTM),[43] a mesoscopic TiO_2 scaffold (m-TiO_2) as a host for the nanostructured perovskite, and a compact TiO_2 film (b-TiO_2) as the hole-blocking layer. The results show significant gains in PV performance from the use of lead iodide perovskites with mixed FA/MA cations as light harvesters.

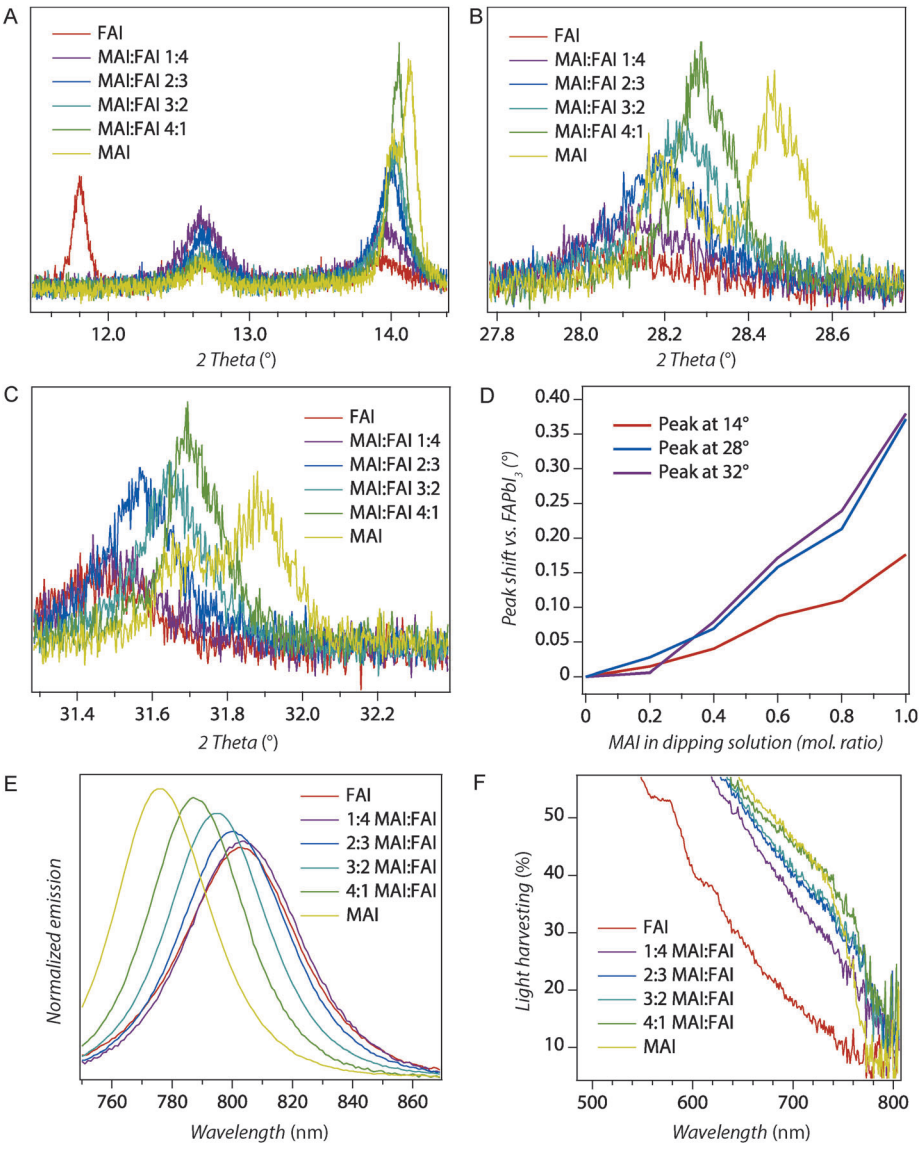

Figure 1. A) XRD characterization of the $(CH_3NH_3)_x(HNCHNH_3)_{1-x}PbI_3$ thin-film perovskites grown by two-step sequential deposition. The substrate was FTO-coated glass on which a typical 300 nm mesoporous TiO_2 scaffold had been deposited. Magnified view of the region 11–14°. The peak at 14.0° shifts to lower reflection angles with FAI intercalation. Remaining PbI_2 was identified at 12.8°. The morphological feature at 11.8° is assigned to the non-perovskite δ-phase of formamidinium. A similar effect is seen in the peaks at B) 31.8° and C) 28.4°. D) Summarized peak shift as compared to $FAPbI_3$. Peaks at 14, 28.4, and 31.8° are considered. E) Normalized emission of $(CH_3NH_3)_x(HNCHNH_3)_{1-x}PbI_3$ ($x=0$, 0.2, 0.4, 0.6, 0.8, 1). The emission is shifted further into the red and broadened as x is decreased. F) Light-harvesting spectra of the different perovskite films recorded in an integrating sphere. Note the 20 nm red shift of the absorbance onset for $(CH_3NH_3)_{0.8}(HNCHNH_3)_{0.2}PbI_3$ as compared to $(CH_3NH_3)PbI_3$. As the formamidinium concentration was increased, the absorbance of the film decreased, while no change in the band gap was discernable.

We conducted powder XRD measurements to investigate the simultaneous intercalation of MA and FA cations (Figure 1). Fluorine-doped tin oxide (FTO) glass was covered with a thin compact blocking layer of TiO_2 (b-TiO_2), onto which mesoscopic TiO_2 (m-TiO_2) with a thickness of approximately 300 nm was deposited. The latter layer was infiltrated with PbI_2 by spin coating, and the resulting material was converted into a mixed-cation perovskite $(MA)_x(FA)_{1-x}PbI_3$ upon exposure to a solution of FAI and MAI in 2-propanol.

Structural changes were observed for the peaks at 14.1 (Figure 1A), 20.0, 24.4, 28.4 (Figure 1B), 31.8 (Figure 1C), 40.6, and 43°, whereby the diffraction angle decreases with increasing formamidinium content, in keeping with the bigger size of the formamidinium cation, which expands the crystal lattice (see Figure SI6 in the Supporting Information for full XRD spectra). Figure 1D shows the peak shift with respect to the reference α-$FAPbI_3$ peak at 13.8°. The gradual shift in the diffraction angle (that is, rather than the appearance of two separate peaks of variable intensities) is a strong indication that a mixed phase of $(MA)_x(FA)_{1-x}PbI_3$ is formed in which the two cations are both inserted in the same lattice frame.

Additional diffractions specific to $FAPbI_3$ appeared at 11.8, 16.25, 30.54, 32.8, and 41.63° and were assigned by measuring spin-coated reference samples produced by the one-step deposition of $(MA)_x(FA)_{1-x}PbI_3$ from *N*,*N*-dimethylformamide (see Figures SI4 and SI5). All of these features were also present in pure $FAPbI_3$ deposited in this way, and are assigned to the yellow δ-phase of $FAPbI_3$.[38] However, the perovskite α-$FAPbI_3$ phase was not produced in this manner, as is evident from the lack of a peak at 14°, and even subsequent annealing failed to induce any δ→α phase transition. The δ-$FAPbI_3$ diffraction peaks gradually disappeared as the MAI concentration was increased. In contrast, the desired black α-$FAPbI_3$ perovskite phase was formed immediately in substantial proportion relative to δ-$FAPbI_3$ when the sequential deposition method was applied. Furthermore, the α-phase was formed quantitatively already at a MAI molar ratio as low as 0.2 in the 2-propanol dipping solution, as confirmed by the lack of a diffraction peak at 11.8°. Yet another key advantage of the two-step over the single-step perovskite deposition method is that it directs perovskite crystallization in the desired α-phase upon exposure of the PbI_2 to the MAI/FAI mixture in 2-propanol.

Since $MAPbI_3$ displays mixed electronic–ionic conduction,[38] we performed impedance analysis and DC polarization to probe electrical transport in the single- and mixed-cation perovskites. AC impedance data acquired for all compositions considered in this study are characterized by a single semicircle (Figure 2A), whereby the capacitance corresponds to the bulk properties (relative dielectric constant $\varepsilon_r \approx 30$). AC measurements performed between 30 and 70 °C yielded the activation energy E_a of the different samples. Remarkably, as shown in Figure 2B, the value of E_a of the two-phase mixtures (e.g. 0.53 eV for MAI:FAI 2:3 as well as MAI:FAI 3:2) is very close to the activation energy of the FAI single phase (0.55 eV) rather than the MAI single phase (0.40 eV), thus suggesting that the electrical conduction properties are dominated by the FAI phase. DC polarization measurements with carbon electrodes revealed a minor but substantial ionic contribution.

Figure 1F shows UV/Vis absorption spectra of the mixed-cation lead iodide perovskites $(MA)_x(FA)_{1-x}PbI_3$ for various compositions. The addition of only 20 mol% FAI to the dipping solution caused the absorption onset of the perovskite to red shift by 20 nm, whereas the desired steepness of the absorption edge characteristic of MAI was maintained. As the FAI concentration was further increased, the absorbance onset was shifted to longer wavelengths, while the absorbance

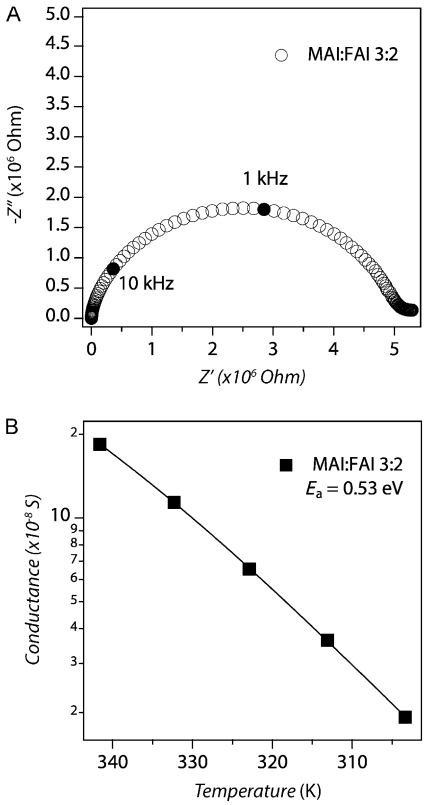

Figure 2. A) AC conductivity of $MA_{0.6}FA_{0.4}PbI_3$ as measured under argon at 70 °C. B) Arrhenius plot of the AC conductance as a function of the temperature for $MA_{0.6}FA_{0.4}PbI_3$.

of the film was reduced. A MAI:FAI ratio of 4:1 or 3:2 in the 2-propanol bath solution proved to be optimal for the extension of the light absorption of the perovskite into the red with retention of the high absorption coefficient of $MAPbI_3$. $MAPbI_3$ scatters light more strongly than $FAPbI_3$, as is apparent from the tailing of the absorbance beyond the band gap. This difference probably arises from the smaller size of $FAPbI_3$ crystals as compared to their methylammonium counterparts.

The normalized near-infrared photoluminescence (PL) of the $(MA)_x(FA)_{1-x}PbI_3$ ($x = 0$–1) films is shown in Figure 1E. A significant 27 nm red shift in the emission peak from $MAPbI_3$ ($\lambda_{max} = 776$ nm) to $FAPbI_3$ ($\lambda_{max} = 803$ nm) was observed—consistent with the absorption spectrum—along with a noticeable broadening of the emission profile. The gradual shift in emission indicates the formation of a solid solution of MA and FA in the perovskite lattice. The shifts in emission of samples prepared by sequential deposition or by single-step deposition are plotted in Figure SI2 of the Supporting Information. The similarity of the observed trends suggests that the ratio of intercalated cations is similar to that of the dissolved cations in the precursor solution. The nonlinearity of the emission shift reflects interactions between methylammonium and formamidinium cations. PL measurements of films prepared by the one-step deposition method were complicated by the appearance of the yellow δ-phase of the formamidinium iodide,[38] which optically manifests itself only weakly in the $FAPbI_3$ samples prepared

by sequential deposition. The absence of the α-phase explains the blue-shifted emission in $FAPbI_3$ prepared by the one-step deposition method (see Figure SI 1).

We measured the current (J)–voltage (V) characteristics of the solar cells in the dark and under simulated air mass 1.5 global standard sunlight (AM 1.5 G). To avoid batch-to-batch variations in the photocurrent, cells from the same batch were compared, and the PbI_2-coated TiO_2 films were selected at random before dipping in the solutions of RNH_3I (R: CH_3– and/or NH=CH–). In this manner, clear trends in the short-circuit current densities were established reproducibly. The dotted trace in Figure 3 A shows a J–V curve for a typical device based on pure $MAPbI_3$, from which the short-circuit current density (J_{sc}), open-circuit potential (V_{oc}), fill factor (FF), and power-conversion efficiency (PCE) were determined to be 17.83 mA cm^{-2}, 1046 mV, 0.655, and 12.5 %, respectively. On average, the devices showed a short-circuit current density of 17.3 mA cm^{-2} and a PCE of 12.0 %, in excellent agreement with our previously reported results.[23] The solid trace in Figure 3 A shows a J–V curve obtained from pure formamidinium lead iodide ($FAPbI_3$) with J_{sc} = 16.6 mA cm^{-2}, V_{oc} = 928 mV, FF = 0.66, and PCE = 10.5 %. The most efficient $FAPbI_3$-based device gave a PCE of 11.0 %, clearly below the average PCE obtained with $MAPbI_3$.

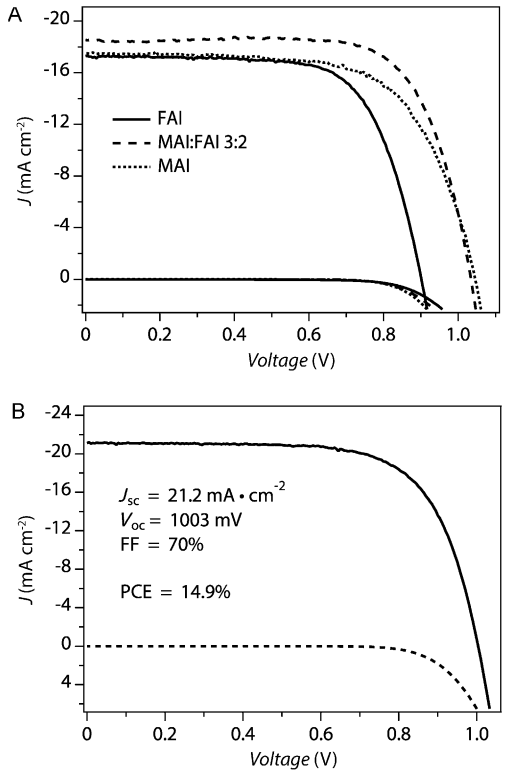

Figure 3. A) J–V curves for average photovoltaic devices assembled with $(CH_3NH_3)_x(HNCHNH_3)_{1-x}PbI_3$ (x = 0, 0.6, 1) as the sensitizer. The performance of the cells was measured in the dark and under a simulated AM 1.5 G spectrum at 98.89, 98.16, and 98.50 mW cm^{-2} for x = 1, 0.6, and 0, respectively. B) J–V curves of the best-performing cell sensitized with $(CH3NH3)_{0.6}(HN{=}CHNH3)_{0.4}PbI_3$, as measured under a simulated AM 1.5 G solar spectrum at 98.2 mW cm^{-2} (solid line) and in the dark (dashed line).

We tested four different mixed-cation perovskites $(MA)_x(FA)_{1-x}PbI_3$ of composition x = 0.2, 0.4, 0.6, and 0.8. Among those, $MA_{0.6}FA_{0.4}PbI_3$ performed best. The dashed trace in Figure 3 A shows the J–V characteristics of a typical cell, with V_{oc} = 1027 mV, J_{sc} = 18.15 mA cm^{-2}, a FF of 0.715, and a PCE of 13.4 %. Strikingly, $MA_{0.6}FA_{0.4}PbI_3$ outperforms the single-cation compositions $MAPbI_3$ and $FAPbI_3$. Figure 3 B shows the J–V characteristics of the best device, which exhibited a J_{sc} value of 21.2 mA cm^{-2}, a V_{oc} value of 1.003 V, and a FF of 0.70 for an overall power-conversion efficiency of 14.9 %. In Table 1 we report the PV characteristics of a series of other cells sensitized by $MA_{0.6}FA_{0.4}PbI_3$.

Table 1: Photovoltaic properties of eight devices sensitized by $MA_{0.6}FA_{0.4}PbI_3$ with $I^{<M->}$ at a concentration of either 0.062 M (first four devices) or 0.050 M (last three devices) in the dipping bath.

J_{sc} [mA cm^{-2}]	V_{oc} [V]	FF	PCE [%]
18.860	1025	0.692	13.71
18.893	1033	0.722	14.52
17.820	1033	0.673	12.93
18.340	1039	0.697	13.57
19.865	931	0.660	12.45
19.617	936	0.696	13.19
19.305	951	0.707	13.39
18.957 ± 0.66	992 ± 46	0.692 ± 0.019	13.4 ± 0.6

To rationalize the substantial gains in photocurrent observed for the mesoscopic cells based on mixed-cation perovskite light harvesters, we measured their incident-photon-to-current conversion efficiency (IPCE), or external quantum efficiency (EQE), across the visible spectrum. Figure 4 B shows that the photocurrent onset is shifted by 20 nm to the red from 780 to 800 nm for $FAPbI_3$ and $MA_{0.6}FA_{0.4}PbI_3$ in accordance with the absorbance spectra shown in Figure 1 F. The IPCE spectrum of $MA_{0.6}FA_{0.4}PbI_3$ is most impressive, as it combines the advantage of the red-shifted onset observed for $FAPbI_3$ with the steep increase in the IPCE at the band gap characteristic for $MAPbI_3$. The IPCE values attained with $MA_{0.6}FA_{0.4}PbI_3$ exceeded the levels of the two single-cation perovskites across the whole visible range and reached close to 90 % at 500 nm. Integration of the IPCE spectra (340–850 nm) over the air mass 1.5 global (AM 1.5 G) solar emission spectrum yielded short-circuit photocurrent densities of 17.0, 16, and 20.2 mA cm^{-2} for $MAPbI_3$, $FAPbI_3$, and $MA_{0.6}FA_{0.4}PbI_3$, respectively.

Figure 4 A shows the absorptance spectra measured with an integrating sphere for the three devices. For this analysis, we removed the gold back contact and cut the films to preserve the active area alone. For wavelengths between 320 and 520 nm, the films harvested more than 93 % of the incident photons. The remaining few percent are transmitted or lost either by specular reflectance or parasitic absorbance by the FTO. Above 520 nm, the light-harvesting efficiency of the films decreases gradually and then dropped sharply to zero near the band gap of the perovskite. $FAPbI_3$ showed the fastest drop in absorbance with increasing wavelength, and $MAPbI_3$ the slowest, while the mixed-cation perovskite lays in-between. A slight red shift in the band gap was observed

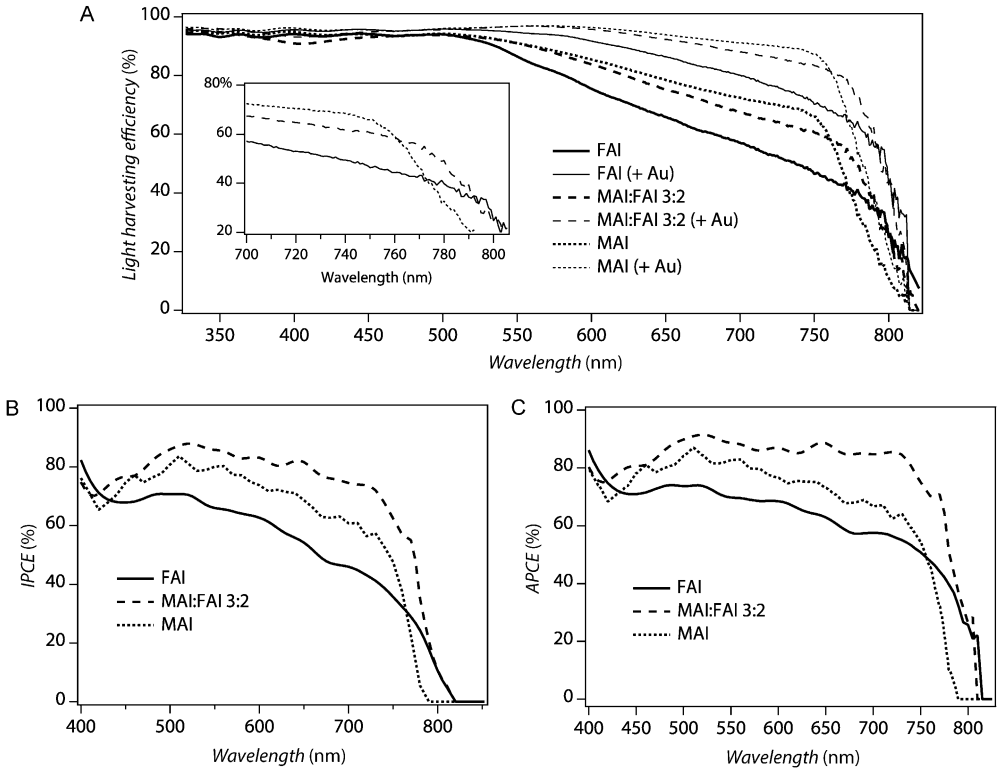

Figure 4. A) Light-harvesting efficiency of $(CH_3NH_3)_x(HNCHNH_3)_{1-x}PbI_3$ ($x = 0$, 0.6, 1). The measurement was performed right after measuring the IPCE and cutting the cell to the active area, after removal of the gold back contact. The measurement was performed in an integrated sphere to account for diffuse reflectance. The sample was placed successively in the beam and perpendicularly to the beam to compensate for secondary absorption. B) IPCE spectrum of the three cells. Note the red-shifted IPCE onset above 800 nm for the mixed-cation perovskite as well as the pure formamidinium lead iodide. C) APCE spectrum derived from the IPCE spectrum and the light-harvesting efficiency.

from the onset of the absorption, that is, 787 nm (1.575 eV) for $MAPbI_3$ and 810 nm (1.530 eV) for $FAPbI_3$. Interestingly, $MA_{0.6}FA_{0.4}PbI_3$ showed the same band gap as $FAPbI_3$, contrary to expectations.

To account for the reflection of the gold counter-electrode, we corrected the absorptance of the films on the basis of the following assumptions: a) the counter-electrode is described by the optical parameters n and k of gold,[44] whereby transmission is neglected and a flat interface is assumed; b) the perovskite film behaves as a Beer–Lambert medium; c) the parasitic absorptions from oxidized spiro-OMeTAD, TiO_2 and FTO are negligible; d) there is no light-scattering perovskite capping layer; and e) spiro-OMeTAD has a refraction index of 1.5 with a negligible imaginary part. By using these approximations, we derived the absorbed-photon-to-current conversion efficiency (APCE) or internal quantum efficiency (IQE) from dividing the IPCE by the absorptance values. Figure 4c shows that for $MA_{0.6}FA_{0.4}PbI_3$, high APCE values of 80–85% were maintained throughout the visible spectrum. These values attest the very high quantum efficiency of carrier generation and collection by the device, in contrast to $MAPbI_3$ and $FAPbI_3$, which seem to collect less charges produced by red than by blue photons, thus indicating a shorter carrier-diffusion length for the single-cation perovskite phases.

To further substantiate this interpretation, we measured the photoluminescence lifetime of the perovskite deposited on nonconductive glass from solutions of MAI/FAI and PbI_2 in *N*,*N*-dimethylformamide (20% wt). The samples were excited by a 406 nm laser diode and their emission recorded at a right angle through a double monochromator. All films were measured over a 200 ns window divided into 1024 channels. Fluorescence lifetimes are displayed in Figure 5 for $(MA)_x(FA)_{1-x}PbI_3$ ($x = 0$, 0.2, 0.4, 0.6, 0.8, 1). The time decay of the fluorescence signals was fit to two or three exponentials; the lifetimes for the three components were in the range of 1–10, 20–70, and 100–300 ns (Table 2). Strikingly, about 85% of the emission of $MA_{0.6}FA_{0.4}PbI_3$ decayed with a long lifetime of 130 ns; thus, the emission

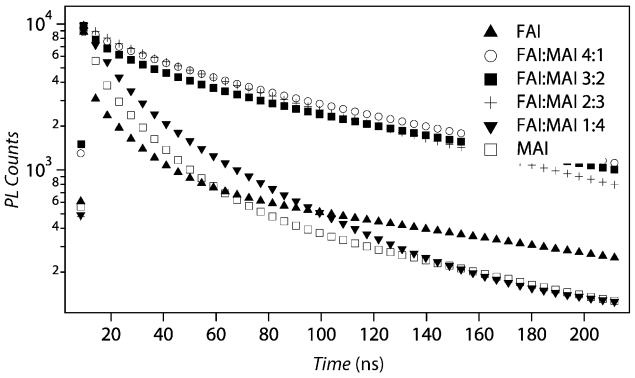

Figure 5. A) Fluorescence lifetime of $(CH_3NH_3)_x(HNCHNH_3)_{1-x}PbI_3$ films spin-coated from a solution of MAI/FAI + PbI_2 in *N*,*N*-dimethylformamide (20% wt). The films were sintered at 80°C for 30 min before the measurement. The signals were fitted to two or three decay exponentials of variable lifetimes.

persisted much longer than for the pure-phase perovskites. It also appears that for the mixed cations, a double exponential is sufficient to fit the decay kinetics well, since the fast decay observed for the single cations is absent. The prolongation of the lifetime in the mixed-cation perovskite most likely contributes to the better carrier-collection efficiency observed

Table 2: Fluorescence lifetime and corresponding intensities for $MAPbI_3$, $FAPbI_3$, and $MA_{0.4}FA_{0.6}PbI_3$ fitted with three exponentials (extracted from the traces in Figure 5).

Lifetime	$MAPbI_3$	$MA_{0.4}FA_{0.6}PbI_3$	$FAPbI_3$
1st	2.58 ns	–	17.3 ns
intensity	11%	–	14%
2nd	17.3 ns	27.6 ns	76.4 ns
intensity	46%	14%	51%
3rd	103 ns	135 ns	173 ns
intensity	43%	86%	35%

with $MA_{0.6}FA_{0.4}PbI_3$, as it enhances the diffusion length of the material.

In summary, we have demonstrated for the first time a perovskite-sensitized photovoltaic device based on the mixed-cation 3D perovskite $(MA)_x(FA)_{1-x}PbI_3$ ($x = 0$–1). The formamidinium cation is presented as a potential replacement for methylammonium in lead iodide perovskites, owing to the red-shifted absorption onset of $FAPbI_3$ as compared to that of $MAPbI_3$. Devices based on $FAPbI_3$ were made by sequential deposition and gave a PCE of 11.0% (a lower value than that of $MAPbI_3$ owing to the presence of the yellow δ-phase). The sequential deposition method and the addition of 20% MA to the FA dipping bath completely avoided the undesirable formation of the δ-phase while maintaining the red-shifted band gap of $FAPbI_3$. The mixed-cation perovskite $MA_{0.6}FA_{0.4}PbI_3$ exhibited superior PV performance to that of the single-cation analogues owing to a greater harvesting and collection of red photons, which resulted in higher short-circuit photocurrents without sacrificing photovoltage. The superior carrier-collection efficiency is probably related to the longer exciton lifetime of more than 130 ns in the $MA_{0.4}FA_{0.6}PbI_3$ material. By using this technique, we were able to fabricate devices yielding up to 14.9% photon-to-current conversion efficiency under the AM1.5G simulated solar spectrum. The strategy of mixing organic ammonium compounds opens up new prospects for the further improvement of the photovoltaic efficiency of perovskite-sensitized solar cells by tuning the optical, electrical, and morphological properties of the semiconducting sensitizer. It is believed that if the formation of the yellow δ-$FAPbI_3$ component could be fully avoided, the performance of pure $FAPbI_3$ would most likely surpass that of $MAPbI_3$-based mesoscopic solar devices. We are currently carrying out studies with this aim.

Received: October 27, 2013
Revised: January 16, 2014
Published online: February 19, 2014

Keywords: energy conversion · light harvesting · organic cations · perovskite solar cells · photovoltaics

[1] G. L. McPherson, J. E. Wall, A. M. Hermann, *Inorg. Chem.* **1974**, *13*, 2230 – 2233.
[2] A. R. Lim, S. H. Kim, *J. Appl. Phys.* **2007**, *101*, 083519.
[3] H. Tanaka, K. Iio, K. Nagata, *J. Magn. Magn. Mater.* **1992**, *104 – 107*, 829 – 830.
[4] C. K. Møller, *Nature* **1958**, *182*, 1436 – 1436.
[5] C. W. M. Timmermans, G. Blasse, *J. Lumin.* **1981**, *24 – 25*, *Part 1*, 75 – 78.
[6] J. Mizusaki, K. Arai, K. Fueki, *Solid State Ionics* **1983**, *11*, 203 – 211.
[7] G. Xing, N. Mathews, S. Sun, S. S. Lim, Y. M. Lam, M. Graetzel, S. Mhaisalkar, T. C. Sum, *Science* **2013**, *342*, 344 – 347.
[8] J. F. Ackerman, G. M. Cole, S. L. Holt, *Inorg. Chim. Acta* **1974**, *8*, 323 – 343.
[9] G. Allan, *Phys. Rev. B* **1990**, *42*, 9174 – 9177.
[10] C. Li, X. Lu, W. Ding, L. Feng, Y. Gao, Z. Guo, *Acta Crystallogr. Sect. B* **2008**, *64*, 702 – 707.
[11] G. L. McPherson, L. J. Sindel, H. F. Quarls, C. B. Frederick, C. J. Doumit, *Inorg. Chem.* **1975**, *14*, 1831 – 1834.
[12] U. Schwarz, F. Wagner, K. Syassen, H. Hillebrecht, *Phys. Rev. B* **1996**, *53*, 12545 – 12548.
[13] L.-C. Tang, C.-S. Chang, J. Y. Huang, *J. Phys. Condens. Matter* **2000**, *12*, 9129 – 9143.
[14] M. Mori, H. Saito, *J. Phys. C* **1986**, *19*, 2391 – 2401.
[15] D.-K. Seo, N. Gupta, M.-H. Whangbo, H. Hillebrecht, G. Thiele, *Inorg. Chem.* **1998**, *37*, 407 – 410.
[16] T. I. Li, G. D. Stucky, G. L. McPherson, *Acta Crystallogr. Sect. B* **1973**, *29*, 1330 – 1335.
[17] D. M. Trots, S. V. Myagkota, *J. Phys. Chem. Solids* **2008**, *69*, 2520 – 2526.
[18] D. B. Mitzi, C. A. Feild, W. T. A. Harrison, A. M. Guloy, *Nature* **1994**, *369*, 467 – 469.
[19] C. R. Kagan, *Science* **1999**, *286*, 945 – 947.
[20] A. Kojima, K. Teshima, Y. Shirai, T. Miyasaka, *J. Am. Chem. Soc.* **2009**, *131*, 6050 – 6051.
[21] N.-G. Park, *J. Phys. Chem. Lett.* **2013**, *4*, 2423 – 2429.
[22] M. M. Lee, J. Teuscher, T. Miyasaka, T. N. Murakami, H. J. Snaith, *Science* **2012**, *338*, 643 – 647.
[23] J. Burschka, N. Pellet, S.-J. Moon, R. Humphry-Baker, P. Gao, M. K. Nazeeruddin, M. Grätzel, *Nature* **2013**, *499*, 316 – 319.
[24] H.-S. Kim, C.-R. Lee, J.-H. Im, K.-B. Lee, T. Moehl, A. Marchioro, S.-J. Moon, R. Humphry-Baker, J.-H. Yum, J. E. Moser, M. Grätzel, N.-G. Park, *Sci. Rep.* **2012**, *2*, 591.
[25] L. Etgar, W. Zhang, S. Gabriel, S. G. Hickey, M. K. Nazeeruddin, A. Eychmüller, B. Liu, M. Grätzel, *Adv. Mater.* **2012**, *24*, 2202 – 2206.
[26] J. Im, J. Chung, S. Kim, N. Park, *Nanoscale Res. Lett.* **2012**, *7*, 1 – 7.
[27] J. H. Heo, S. H. Im, J. H. Noh, T. N. Mandal, C. Lim, J. A. Chang, Y. H. Lee, H. Kim, A. Sarkar, M. K. Nazeeruddin, M. Grätzel, S. I. Seok, *Nat. Photonics* **2013**, *7*, 486 – 491.
[28] D. B. Mitzi, *Chem. Mater.* **1996**, *8*, 791 – 800.
[29] D. B. Mitzi, C. D. Dimitrakopoulos, L. L. Kosbar, *Chem. Mater.* **2001**, *13*, 3728 – 3740.
[30] X. Hong, T. Ishihara, A. Nurmikko, *Phys. Rev. B* **1992**, *45*, 6961 – 6964.
[31] S. Wang, D. B. Mitzi, C. A. Feild, A. Guloy, *J. Am. Chem. Soc.* **1995**, *117*, 5297 – 5302.
[32] D. B. Mitzi, K. Chondroudis, C. R. Kagan, *Inorg. Chem.* **1999**, *38*, 6246 – 6256.
[33] D. B. Mitzi, *Inorg. Chem.* **2000**, *39*, 6107 – 6113.
[34] D. B. Mitzi, P. Brock, *Inorg. Chem.* **2001**, *40*, 2096 – 2104.
[35] I. Borriello, G. Cantele, D. Ninno, *Phys. Rev. B* **2008**, *77*, 235214.
[36] J. L. Knutson, J. D. Martin, D. B. Mitzi, *Inorg. Chem.* **2005**, *44*, 4699 – 4705.
[37] E. Mosconi, A. Amat, M. K. Nazeeruddin, M. Grätzel, F. De Angelis, *J. Phys. Chem. C* **2013**, *117*, 13902 – 13913.
[38] C. C. Stoumpos, C. D. Malliakas, M. G. Kanatzidis, *Inorg. Chem.* **2013**, *52*, 9019 – 9038.
[39] W. Shockley, H. J. Queisser, *J. Appl. Phys.* **1961**, *32*, 510.
[40] D. Mitzi, S. Wang, C. Feild, C. Chess, A. Guloy, *Science* **1995**, *267*, 1473 – 1476.

[41] Y. Lee, D. Mitzi, P. Barnes, T. Vogt, *Phys. Rev. B* **2003**, *68*, 020103.
[42] J. H. Noh, S. H. Im, J. H. Heo, T. N. Mandal, S. Il Seok, *Nano Lett.* **2013**, *13*, 1764 – 1769.
[43] J. Burschka, A. Dualeh, F. Kessler, E. Baranoff, N.-L. Cevey-Ha, C. Yi, M. K. Nazeeruddin, M. Grätzel, *J. Am. Chem. Soc.* **2011**, *133*, 18042 – 18045.
[44] *Handbook of Optical Constants of Solids*, *Vol. 1* (Ed.: E. D. Pallik), Academic Press, San Diego, **1985**.
[45] J.-H. Im, C.-R. Lee, J.-W. Lee, S.-W. Park, N.-G. Park, *Nanoscale* **2011**, *3*, 4088 – 4093.

